

1 **Disruption in structural-functional network repertoire and time-**  
2 **resolved subcortical-frontoparietal connectivity in disorders of**  
3 **consciousness**

4 *Rajanikant Panda<sup>1,2</sup>, Aurore Thibaut<sup>1,2</sup>, Ane Lopez-Gonzalez<sup>3</sup>, Anira Escrichs<sup>3</sup>, Mohamed Ali*  
5 *Bahri<sup>1,2</sup>, Arjan Hillebrand<sup>4</sup>, Gustavo Deco<sup>3</sup>, Steven Laureys<sup>1,2</sup>, Olivia Gosseries<sup>1,2</sup>, Jitka*  
6 *Annen<sup>\*1,2</sup>, Prejaas Tewarie<sup>\*4,5</sup>*

7 <sup>1</sup> *Coma Science Group, GIGA-Consciousness, University of Liege, Liege, Belgium*

8 <sup>2</sup> *Centre du Cerveau<sup>2</sup>, University Hospital of Liege, Liege, Belgium*

9 <sup>3</sup> *Computational Neuroscience Group, Center for Brain and Cognition, Universitat Pompeu*  
10 *Fabra, Barcelona, Spain*

11 <sup>4</sup> *Amsterdam UMC, Vrije Universiteit Amsterdam, Department of Clinical Neurophysiology*  
12 *and MEG Center, Amsterdam Neuroscience, Amsterdam, The Netherlands*

13 <sup>5</sup> *Sir Peter Mansfield Imaging Centre, School of Physics and Astronomy, University of*  
14 *Nottingham, Nottingham, United Kingdom*

15

16 \* Equal contribution

17 Page count: 23

18 Figures: 4

19

20

21

22

23 Corresponding author:

24 Prejaas Tewarie, MD, PhD

25 Department of Clinical Neurophysiology and MEG Center

26 Amsterdam UMC, Vrije Universiteit Amsterdam, Amsterdam Neuroscience

27 Amsterdam

28 The Netherlands

29 Email: p.tewarie@amsterdamumc.nl

30

31

32 **Abstract**

33 Understanding recovery of consciousness and elucidating its underlying mechanism is  
34 believed to be crucial in the field of basic neuroscience and medicine. Ideas such as the global  
35 neuronal workspace and the mesocircuit theory hypothesize that failure of recovery in  
36 conscious states coincide with loss of connectivity between subcortical and frontoparietal  
37 areas, a loss of the repertoire of functional networks states and metastable brain activation.  
38 We adopted a time-resolved functional connectivity framework to explore these ideas and  
39 assessed the repertoire of functional network states as a potential marker of consciousness  
40 and its potential ability to tell apart patients in the unresponsive wakefulness syndrome (UWS)  
41 and minimally conscious state (MCS). In addition, prediction of these functional network states  
42 by underlying hidden spatial patterns in the anatomical network, i.e. so-called eigenmodes,  
43 were supplemented as potential markers. By analysing time-resolved functional connectivity  
44 from fMRI data, we demonstrated a reduction of metastability and functional network repertoire  
45 in UWS compared to MCS patients. This was expressed in terms of diminished dwell times  
46 and loss of nonstationarity in the default mode network and fronto-parietal subcortical network  
47 in UWS compared to MCS patients. We further demonstrated that these findings co-occurred  
48 with a loss of dynamic interplay between structural eigenmodes and emerging time-resolved  
49 functional connectivity in UWS. These results are, amongst others, in support of the global  
50 neuronal workspace theory and the mesocircuit hypothesis, underpinning the role of time-  
51 resolved thalamo-cortical connections and metastability in the recovery of consciousness.

52

53

54

55

56

## 57 I. Introduction

58 Diagnosis of the level of consciousness after coma due to severe brain injury is a well-known  
59 dilemma in the field of neurology and intensive care medicine. Coma after cardiac arrest or  
60 after traumatic brain injury (TBI) may result in sustained altered states of consciousness.  
61 These patients with disorders of consciousness (DOC), irrespective of the aetiology, can be  
62 grouped into the unresponsive wakefulness syndrome (UWS) (1), characterized by the  
63 presence of eye-opening and reflexive behaviours, and the minimally conscious state (MCS),  
64 characterized by consistent but fluctuant wilful conscious behaviours, such as command  
65 following or visual pursuit (2, 3). Recovery of consciousness is argued to emerge conjointly  
66 with restoration of resting-state functional brain networks (4), which refers to patterns of  
67 neuronal interactions inferred by indirect (e.g., functional magnetic resonance imaging - fMRI)  
68 or direct (e.g., electro- and magneto-encephalography (EEG/MEG)) measurements. Analysis  
69 of these resting-state networks could potentially help in the diagnosis of patients with DOC  
70 and provide insight into the mechanisms that results in absence of recovery of consciousness  
71 in UWS.

72 Various resting-state networks that play an important role in the recovery of consciousness  
73 have been identified, among which the default mode network (DMN), fronto-parietal network  
74 (FPN) and the salience network are the most important (5, 6). Recovery of the DMN in  
75 combination with recovery of the auditory network could for instance discriminate between  
76 MCS and UWS with a very high accuracy (~85%) (7). The mechanism of resting-state network  
77 restoration in DOC is yet unknown, however, thalamic activity and especially thalamocortical  
78 connectivity may be a driving force behind restorations of cortical network function that  
79 sustains conscious states (8, 9). Previous work on resting-state networks in DOC have mainly  
80 focused on the “static” picture of functional connectivity (4, 6, 10, 11), i.e., connections are  
81 assessed over the entire duration of the (fMRI) recording and fluctuations in connectivity over  
82 time are ignored. However, the underlying dynamics of connectivity seem relevant for  
83 consciousness (12, 13) and a static description may therefore be inadequate to provide  
84 mechanistic insight into failure of recovery of consciousness in DOC (14).

85 The analysis of dynamic or time-resolved functional connectivity, as well as the relationship  
86 between the underlying anatomical connections and emergent time-resolved functional  
87 connectivity (15, 16), may be clinically relevant in patients with DOC. Previous studies have  
88 already explored the role of time-resolved functional connectivity in DOC (17–19). A recent  
89 study demonstrated that network states with long distance connections occurred less  
90 frequently over time in MCS compared to UWS patients (14), emphasizing disintegration of  
91 interactions across the cortex in unconscious states. However, network states reminiscent of  
92 the well-known resting-state networks were not retrieved. Cao and colleagues used two  
93 methods to extract time-varying networks, i.e. independent component analysis and hidden  
94 Markov modelling, and revealed clinically relevant differences in network state durations  
95 between patients with DOC patients and healthy subjects (20), while lacking comparative  
96 analysis between patients in MCS and in UWS. In another fMRI study, the authors focused on  
97 the posterior cingulate area and the DMN using a spatiotemporal point process analysis and  
98 demonstrated decreased occurrence of DMN-like patterns in UWS. Dynamic connectivity  
99 analysis has recently also been applied to EEG data, revealing loss of network integration and  
100 increased network segregation in DOC patients (21). Despite the importance of the previously  
101 published work, the role of the well-known resting-state networks and especially thalamo-  
102 cortical functional connections (22) within the context of time-resolved connectivity and DOC  
103 has so far not been fully explored, partly potentially due to the fact that previous work has  
104 been mostly hypothesis driven rather than data driven.

105 Another important aspect in the context of the emergence or restoration of resting-state  
106 networks is the underlying structural network, as anatomical connectivity patterns influence  
107 the repertoire of possible functional network states (23). It is widely assumed that switching

108 between functional network states is achieved by so-called metastability in the brain (24), i.e.,  
109 winnerless competitive dynamics. A promising and robust approach to analyse the relationship  
110 between structural and functional network states is the so-called eigenmode approach (25–  
111 27). With this approach, spatial harmonic components or eigenmodes are extracted from the  
112 anatomical network. These eigenmodes can be considered as patterns of ‘hidden  
113 connectivity’, which allow for prediction of the well-known resting-state networks (28). It can  
114 be hypothesized that switching between functional network states, as can be observed in the  
115 metastable brain, is accompanied by fluctuations in the expression of eigenmodes (29);  
116 therefore, a potential loss of metastability in DOC could co-occur with loss of modulations in  
117 eigenmode expression (12).

118 In this context, the aim of the current study was fourfold. First, we first tested whether loss of  
119 metastability and resting-state network activity, derived from time-resolved estimates of  
120 functional connectivity, could differentiate between MCS and UWS, with a potential extraction  
121 of a spatiotemporal thalamocortical network state. Second, we analysed whether time-  
122 resolved connectivity could be explained by modulations in expression of eigenmodes in DOC,  
123 and third, whether potential differences in eigenmode expression in DOC patients would co-  
124 occur with a loss of metastability. Finally, we used a classification procedure to evaluate  
125 whether the collection of these network-based measures could predict patients’ diagnosis.

## 126 **II. Results**

127 We included 34 healthy control subjects (HC, 39 (mean)  $\pm$  14 years (standard deviation), 20  
128 males), 30 MCS (41  $\pm$  13 years, 21 males) and 14 UWS patients (48  $\pm$  16 years, 7 males).  
129 There was no difference in the age of patients with MCS and UWS ( $p > 0.05$ ), gender ( $p >$   
130  $0.05$ ), time since injury ( $p > 0.05$ ) and aetiology ( $p > 0.05$ ). There was also no difference in  
131 age ( $p > 0.05$ ) and gender ( $p > 0.05$ ) between HC and DOC patients. Further details about the  
132 patient population is described in the methods and supplementary table 1.

### 133 *Metastability and time-resolved functional connectivity in patients with DOC*

134 Time-resolved or dynamic connectivity for all subjects was extracted from the phase  
135 information of the data. We quantified a proxy measure for metastability defined as the  
136 standard deviation of the overall phase behaviour over time (i.e. the Kuramoto order  
137 parameter). This was followed by extraction of spatiotemporal patterns using non-negative  
138 tensor factorisation (NNTF) from phase connectivity data, corresponding to resting-state  
139 networks or network states (see Figure 1). Well-known resting-state networks as well as a  
140 residual component were used as initial conditions for the spatial connectivity patterns for all  
141 network states to allow for stable convergence of the algorithm (i.e. DMN, FPN, visual network,  
142 sensorimotor network, salience network, subcortical network (30)). However, the NNTF  
143 algorithm allowed the spatial patterns of these network states to change in order to maximize  
144 the explained variance of the data. Temporal statistics from the network states were derived  
145 for every network state in terms of excursions from the median (proxy for nonstationarity (31)  
146 and state duration (i.e., dwell time).

147 A reduction of metastability was found in DOC patients compared to HCs (Figure 2A). Lower  
148 metastability was observed in UWS patients in comparison to MCS patients (Figure 2A).  
149 Reduced metastability is expected to occur with loss of switching between resting-state  
150 networks and potentially with dwelling within a more limited subset of resting-state networks  
151 in DOC. The output of the NNTF algorithm resulted in spatial topographies of some of the well-  
152 known resting-state networks, i.e., the default mode network (DMN), a separate posterior DMN  
153 around the precuneus, the visual network, the salience network (SN), the fronto-parietal  
154 network (FPN), and a network consisting of fronto-parietal and subcortical regions (FPN-sub)  
155 (Figure 2 I-N). Note that these network states were not identical to the initial conditions, e.g.  
156 the subcortical network that was provided as initial condition to NNTF was incorporated with

157 the frontoparietal network (Figure 2N) by the NNTF algorithm. At the same time, the  
158 sensorimotor network that was provided as initial condition disappeared as state. Excursions  
159 from the median were lower for most networks (DMN, visual, Salience, Posterior DMN and  
160 FPN-sub) in DOC compared to HC (Figure 2 C-F, H). Significant loss of nonstationarity was  
161 also found in UWS compared to MCS for the DMN, FPN, FPN-sub (Figure 2 C,G,H). The  
162 NNTF also yielded a residual state, with a lack of spatial structure, accounting for the variance  
163 of connectivity data not explained by the resting-state networks. The residual component had  
164 longer dwell times for the decreasing levels of consciousness (Figure 2B). In addition, as in  
165 line with the metastability results, there were lower dwell times in DOC patients for a specific  
166 set of resting-state networks (Salience, Posterior DMN, FPN and FPN-sub), and dwell time  
167 was shorter in UWS patients compared to MCS patients only in the FPN-sub network (see  
168 results in Figure S1).

### 169 *Relationship between structural eigenmodes and time-resolved functional connectivity in DOC*

170 We next analysed how disruption in time-resolved functional connectivity in DOC was related  
171 to the underlying structural network. In order to put our findings into context, we first analysed  
172 the relationship between static functional networks and structural networks, using the Pearson  
173 correlation between static functional connectivity and structural connectivity for the different  
174 groups (Figure 3A). These results show that functional connectivity in DOC patients show  
175 more correspondence with the underlying structural connectivity as compared to HCs, as the  
176 relationship between structural and functional connectivity was stronger for decreasing levels  
177 of consciousness (Figure 3A).

178 We next obtained the eigenmodes from the structural connectivity by extracting the  
179 eigenvectors of the graph Laplacian. These eigenmodes can be regarded as distinct spatial  
180 harmonics within the structural connectivity, where the first eigenmodes correspond to  
181 patterns with low spatial frequency and subsequent eigenmodes contain patterns with  
182 increasingly higher spatial frequencies. Given their spatial configuration, consecutive  
183 eigenmodes can be associated with increasing levels of segregation while the first  
184 eigenmodes can be linked with network integration. For every time point we predicted the  
185 extent to which phase connectivity could be explained by a weighted combination of the  
186 eigenmodes (27). Since phase connectivity can evolve over time, the weighting coefficients  
187 for the eigenmodes can modulate as well, resulting in fluctuations in the strength of the  
188 expressions of eigenmodes over time. For every eigenmode, we could then quantify the  
189 modulation strength (i.e. how much the eigenmode-expression varied over time). In addition  
190 to the weighting coefficients, we also obtain the goodness-of-fit for the predictions of time-  
191 resolved functional connectivity.

192 The goodness-of-fit for the eigenmode predictions is displayed in Figure 3B, where we show  
193 the average correlation between eigenmode predicted FC and empirical FC for the three  
194 groups. Results show better predictions for HC and MCS compared to predictions for static  
195 FC (median and interquartile range of correlations HC static  $0.18 \pm 0.04$ , HC eigenmode  $0.39$   
196  $\pm 0.09$ ,  $Z = -7.1$ ,  $p < 0.001$ , MCS static  $0.2 \pm 0.05$ , MCS eigenmode  $0.35 \pm 0.18$ ,  $Z = -4.8$ ,  $p <$   
197  $0.001$ ). In order to test whether these eigenmode predictions of time-varying connectivity could  
198 have been obtained by chance, we redid our analysis using surrogate BOLD data (see method  
199 section "Analysis steps"). Results showed that eigenmode predictions for time-resolved  
200 connectivity from surrogate data performed significantly worse compared to genuine empirical  
201 data (for all comparisons with surrogate data  $p < 0.001$ ; Figure 3B). We did not test whether  
202 contribution of individual eigenmodes differed between groups as this would come with a  
203 serious multiple comparisons problem.

204 Instead, since structural connectivity appeared to correlate stronger with static FC in DOC  
205 compared to HC, we expected that eigenmode coefficients in DOC patients would hardly  
206 change over time, underlining the observation of a 'fixed' structural-functional network

207 relationship in DOC patients. To analyse this lack of change in the structural-functional  
208 network relationship over time in DOC patients, we quantified the modulation strength of the  
209 weighting coefficients over time (see methods “*Analysis steps*”). We performed this analysis  
210 separately for the dominant (1<sup>st</sup> to 107<sup>th</sup> eigenmode, first half) and non-dominant eigenmodes  
211 (108<sup>th</sup> to 214<sup>th</sup> eigenmode, second half). Results for the dominant eigenmodes show a clear  
212 reduction in modulation of the eigenmode weighting in DOC patients compared to HCs (Figure  
213 3C), with also a significantly lower modulation of eigenmode expression in UWS compared to  
214 MCS patients. This result could not be explained by chance, since the same results could not  
215 be obtained from surrogate data (Figure 3C). Note that no between group difference for non-  
216 dominant eigenmodes was obtained (Figure 3D).

217 We have so far shown a reduction in modulation strength of eigenmode expressions in DOC  
218 patients compared to HC subjects, as well as a loss of metastability in DOC patients and  
219 dwelling of the brain in fewer network states in DOC patients. This poses the question whether  
220 these two observations are related. In Figure 3EFG we show that metastability is strongly  
221 correlated to modulations in eigenmode expression within every group. This underscores the  
222 notion that loss of dynamic modulations in functional network patterns due to a loss of  
223 metastability could indeed be related to a reduced modulation of eigenmode expression.

#### 224 *Classification of DOC patients using measures of dynamic functional connectivity and* 225 *structure-function relationships*

226 To translate the structural and functional dynamic properties of the brain to clinical practice,  
227 we used a classification approach for functional and structural properties using two class  
228 support vector machine (SVM) classifiers. Only functional and structural properties that  
229 showed group differences were used as features. We used three different classification  
230 approaches of SVM (i.e., leave one out cross validation (LOOCV), k-fold cross validation, and  
231 splitting the data into 60-40% training and testing data respectively). The LOOCV showed  
232 better performance in terms of classification between groups for the selected features,  
233 compared to the other approaches (see Table 1). Using LOOCV, UWS versus MCS  
234 classification accuracy was 79.1%, with a sensitivity of 83.3% and specificity of 69.2%. When  
235 we compared healthy controls with the DOC patient group, the classification performance was  
236 very high. For healthy controls versus UWS, we found a classification accuracy of 95.8%, with  
237 a sensitivity of 97.1% and a specificity of 92.3%. The healthy controls versus MCS  
238 classification accuracy was 95.3%, with a sensitivity of 94.1% and specificity of 96.7% (Table  
239 1). We also used the surrogate data to assess whether such a classification accuracy could  
240 be obtained by chance. We found that the classification algorithm assorted all subjects into  
241 one group, with an accuracy equal to chance level, a sensitivity of 100% and specificity of 0%  
242 (Table 1). These results indicate that the classification performance of functional and structural  
243 features is beyond chance level.

244 To further understand which features were most discriminating between UWS and MCS, we  
245 used a feature ranking based on diagonal adaptation of neighbourhood component analysis  
246 (NCA). Results showed that the most important features were nonstationarity in the DMN  
247 (feature weight (FW)=2.22), Salience network (FW=1.03), FPN (FW=0.66), visual network  
248 (FW=0.18), FPN-sub network (FW=0.1). Remaining features had low feature weights (<0.01)  
249 (Figure 4). Interestingly we found that purely structural features had very low weights,  
250 indicating that purely structural properties contribute very little beyond functional features to  
251 the classification between UWS versus MCS, as well as between healthy controls versus DOC  
252 patients.

253

### 254 III. Discussion

255 Differentiation between MCS and UWS is key for adequate diagnosis and prognosis in DOC  
256 patients as this is connected to medical-ethical end of life decisions. Use of imaging  
257 characteristics allows testing of hypotheses on causes for delayed, or failure of, recovery of  
258 consciousness. Here, we used state-of-the art techniques to quantify time-varying functional  
259 connectivity, metastability and the relationship between the underlying anatomical network  
260 and time-resolved functional connections. We demonstrated that these advanced techniques  
261 were sensitive to detect clinically relevant differences for the diagnosis of MCS and UWS  
262 patients. More specifically, we first demonstrated that UWS patients show reduced  
263 metastability, and spend less time in states outside the natural equilibrium state that would  
264 favor cerebral processing in a cooperative and coordinated manner to support consciousness.  
265 This is accompanied by shorter state durations that the brain spends in the frontoparietal-  
266 subcortical configuration in UWS. A loss of nonstationarity was observed in several resting-  
267 state networks (i.e., DMN, frontoparietal and frontoparietal-subcortical) in UWS compared to  
268 MCS patients. We furthermore showed that functional brain networks are more 'fixed' to the  
269 underlying anatomical connections and are less subject to spatial reconfigurations over time  
270 in UWS compared to MCS patients. The extent to which these spatial reconfigurations  
271 occurred (i.e., expressed as modulations in eigenmode-expression) correlated strongly to  
272 metastability. Lastly, classification analysis showed that out of all results, nonstationarity in the  
273 DMN, salience network, frontoparietal network, visual network and in the frontoparietal-  
274 subcortical network were features that were most discriminating between MCS and UWS.

275 Our results are in agreement with several hypothesis and theories for the emergence of  
276 consciousness, of which most share the importance of thalamocortical connectivity for  
277 consciousness (32–34). The mesocircuit hypothesis states that deafferentation between the  
278 frontal cortex and subcortical regions is crucial in explaining failure of recovery of  
279 consciousness (32). One of the most novel findings in the current work is the generation of  
280 the frontoparietal-subcortical network. Although subcortical connections were, among others,  
281 used as initial conditions for the decomposition of the time-varying functional connectivity  
282 patterns into resting-state networks, incorporation with fronto-parietal connections emerged  
283 from the data-driven NNTF algorithm. Another observation confirms that this NNTF approach  
284 was extracting DOC-relevant networks, namely that the sensorimotor network disappeared  
285 after optimization of spatial network patterns. This latter result is in line with the fact that  
286 somatosensory cortices are not directly involved in the emergence of consciousness, based  
287 on current theories (35). In addition, we found that the frontoparietal-subcortical network  
288 showed shorter dwell times in DOC patients compared to HC subjects, with even shorter state  
289 durations in UWS compared to MCS patients. Finally, this network also demonstrated a loss  
290 of nonstationarity in UWS compared to MCS patients. However, it should be noted that the  
291 frontoparietal-subcortical network was not the only network with loss of time-resolved network  
292 characteristics; other resting-state networks also showed loss of nonstationarity, such as the  
293 DMN and frontoparietal network. Yet a combination of shorter dwell times and loss of  
294 nonstationarity was only found for the frontoparietal-subcortical network. The mesocircuit  
295 hypothesis suggests that lack of excitation of the inhibition of the thalamus induces a reduction  
296 of thalamo-cortical connectivity, which in turn, causes a reduction of the activity in the whole  
297 frontoparietal network. It may be tempting to interpret that the frontoparietal-subcortical  
298 network may play a crucial role in orchestrating global network interactions and dwell times.  
299 Hence, this sub-network may be instrumental for the observed loss of nonstationarity in the  
300 other sub-networks. Although the importance of functional connections between the thalamus  
301 and frontal cortex has been emphasized by the mesocircuit hypothesis, and shown to relate  
302 to consciousness in hypothesis-driven functional (e.g., (8, 22, 36)) and structural (e.g., (37,  
303 38)) neuroimaging studies, this is the first demonstration of the ability of a (semi)data-driven  
304 approach to identify this sub-network in the context of time-resolved functional connectivity.  
305 Most previous data-driven approaches have been unable to extract such a network (14, 20,  
306 21).

307 Our findings also support the global neuronal workspace (GNW) theory (33), which  
308 emphasizes the importance of long-distance and recurrent functional connections, large-scale  
309 reverberant networks and metastable brain states in the emergence and recovery of  
310 consciousness (39). So far, the importance of metastability has mainly been addressed in the  
311 context of recovery of consciousness from anesthesia (40). Here, we underscore this finding  
312 and demonstrate that a reduction of metastability can even differentiate between UWS and  
313 MCS patients. We further show that in DOC patients, the brain is dwelling shorter in relevant  
314 and important network states, indicating that a more limited repertoire of functional network  
315 states in DOC patients. There is still some dwelling time in the DMN, salience network, visual  
316 network and in the unstructured residual state, but shorter dwell time in especially the  
317 frontoparietal and frontoparietal-subcortical network.

318 Diagnosis and prognosis of patients in DOC is challenging and merely relying on clinical  
319 measures may be unreliable (41, 42). Specialistic imaging techniques such as positron  
320 emission tomography (PET) have shown their added-value to complement the clinical  
321 diagnosis of DOC patients (4). Especially the lack of activation of a frontoparietal-subcortical  
322 network in UWS has been postulated by several hypotheses on DOC (4). Here, we have used  
323 a non-invasive imaging protocol and demonstrated the role of time-resolved functional  
324 connectivity and disrupted structural-functional network coupling to differentiate between MCS  
325 and UWS patients. Our findings allow differentiation between MCS and UWS with about 80%  
326 accuracy, commensurate with previous work (7, 37, 43, 44). A high sensitivity (83%, i.e., true  
327 positive for the presence of consciousness) and slightly lower specificity (69%, i.e., true  
328 negative predicting the absence of consciousness) was obtained. This might reflect the finding  
329 that behavioural assessment might underestimate the presence of consciousness in up to 2/3  
330 of the UWS patients (45). Since our sample size was limited with only 14 UWS patients, we  
331 did not use a separate validation dataset to verify our classification results. Instead, we applied  
332 a few different approaches to verify our results and we used surrogate data to find out whether  
333 our classification could have been obtained by chance. This was not the case. Diagnosis in  
334 itself was not the sole goal of the classification analysis, but the adopted approach also aided  
335 to elucidate mechanisms that would lead to (failure of) recovery of consciousness in DOC  
336 leveraging the data-driven obtained features. Loss of nonstationarity in the DMN, salience  
337 network and frontoparietal turned out to be important discriminating features to tell apart MCS  
338 and UWS.

339 Our observation of functional connectivity dynamics that are more restricted to the structural  
340 connectivity has been observed in pharmacological and pathological loss of consciousness  
341 (see also (14, 46)), however, here we show that this co-occurred with a reduction of  
342 metastability. Previous work has demonstrated that the underlying anatomical connectivity  
343 forms a constraint for functional connectivity and also shapes the repertoire of possible  
344 functional network states (24). The underlying anatomical connectivity contains so-called  
345 inherent 'hidden patterns' or eigenmodes with different spatial structures. In a dynamical  
346 system such as the brain, these eigenmodes, or a combination of eigenmodes, can  
347 sequentially be activated or deactivated (25, 47), and thereby shape the repertoire of possible  
348 functional network states. We stress that this framework does not imply that there is some  
349 fixed relationship or coupling between structure and function, but rather that parts of the  
350 anatomical network support the (sequential) formation of specific functional sub-networks, and  
351 not only at the level of individual nodes (46). Although the mechanism behind the  
352 (de)activation of these spatial eigenmodes remains to be investigated, we posit that a potential  
353 underlying mechanism for a loss of the functional repertoire in DOC is the inability to  
354 sequentially dwell for prolonged times in a different set of eigenmodes. This inability was even  
355 more pronounced for UWS than for MCS.

356 A few methodological aspects in our retrospective study deserve further discussion. First of  
357 all, we did not analyse the contributions of individual eigenmodes for two reasons: i) although  
358 earlier studies have demonstrated that a limited set of eigenmodes could already explain

359 observed functional connectivity pattern (25), in our case, assessing group differences  
360 between MCS and UWS on the basis of individual eigenmodes would impose a multiple  
361 comparisons problem; ii) our analytical approach is based on the assumption that all  
362 eigenmodes are necessary in the mapping to functional connectivity instead of a statistical  
363 selection of eigenmodes. Second, using fMRI to look at dynamic FC, and particular phase-  
364 based FC, may not be optimal. High temporal resolution of EEG/MEG may be able to provide  
365 even more reliable estimates of dynamic FC (even of subcortical structures (48) and on the  
366 relation between SC and dynamic FC (47). Last, concatenated data from all groups were fed  
367 into the NNTF analysis, instead of per group. This assumes that spatial network structure is  
368 similar across groups. Even though this is not necessarily the case, the amount of data to  
369 allow for stable NNTF results for individual groups was limited, especially for the UWS group.  
370 Future (multicentric) studies with more patients should verify whether the decomposition of  
371 the dynamic functional connectivity patterns into the observed sub-networks holds for the  
372 separate groups. Our approach to concatenate data from all groups made group comparison  
373 much easier though, as there was now no need to 'match' potentially slightly different networks  
374 from the different groups. This also allowed us to focus on networks that were important in  
375 DOC.

376 Taken together, we have demonstrated that a (semi) data-driven approach has extracted  
377 clinically meaningful time-resolved functional brain networks. This unique network-based  
378 spatiotemporal characterization accounts for structure-function coupling (i.e., eigenmodes),  
379 and shows a relationship with brain stability. The measures that differed between UWS and  
380 MCS patients most, were the dominant eigenmodes (reflecting structure-function coupling)  
381 and time-resolved functional connectivity in the default mode network, frontoparietal network  
382 and the subcortical-frontoparietal network. Interestingly, the latter network was generated by  
383 the (semi)data-driven approach to better fit the data, and was to sole network to show shorter  
384 dwell times in UWS than MCS patients. This suggests that the subcortical-frontoparietal  
385 network might play a pivotal role for supporting conscious network interactions, as is in line  
386 with several theoretical and hypothesis-driven studies. Future work will be required to assess  
387 to what extent these advanced aspects of connectivity can serve as biomarkers to aid  
388 diagnosis and prognosis in DOC.

## 389 **V. Methods**

### 390 *Participants*

391 Forty-four adult DOC patients, of whom 30 in Minimally Conscious State (MCS) (11 females,  
392 age range 24-83 years; mean age  $\pm$  SD, 45  $\pm$  16 years) and 14 with the Unresponsive  
393 Wakefulness Syndrome (UWS) (6 females, age range 20-74 years; mean age  $\pm$  SD, 47  $\pm$  16  
394 years) and thirty-four age and gender matched healthy subjects (HC) (14 females, age range  
395 19-72 years; mean age  $\pm$  SD, 40  $\pm$  14 years) without premorbid neurological problems were  
396 included. The local ethics committee from the University Hospital of Liège (Belgium) approved  
397 the study. Written informed consent was obtained from all healthy subjects and the legal  
398 representative for DOC patients. The same data was used in (46, 49).

399 The diagnosis of the DOC patients was confirmed through two gold standard approaches (i.e.,  
400 (i) behavioural and (ii) fluorodeoxyglucose-positron emission tomography (FDG-PET),  
401 excluding patients for whom these two diagnostic approaches disagreed. (i) Patients were  
402 behaviourally diagnosed through the best of at least five coma recovery scale revised CRS-  
403 R assessments, evaluating auditory, visual, motor, oromotor function, communication and  
404 arousal (50). (ii) Behavioural diagnosis was complemented with the visual assessment of  
405 preserved brain metabolism in the frontoparietal network using FDG-PET as a neurological  
406 proxy for consciousness (41). Patient-specific clinical information is presented in Table 1. We  
407 only included patients for whom (1) MRI data were recorded without anaesthesia (2) diagnosis

408 was based on at least 5 repetitions of the CRS-R assessment, (3) diagnosed as UWS or MCS,  
409 and (4) the FDG-PET diagnosis was in agreement with the clinical diagnosis. We excluded  
410 the patients (1) for whom the patients the structural MRI segmentation was incorrect or (2) if  
411 there were excessive head movement artefacts during MR recordings. There were 46 MCS  
412 patients in which 16 were discarded due to mismatch of PET and CRS-R diagnosis, 8 for failed  
413 segmentation and 4 for head movement artefacts. Amongst the 28 UWS patients, 8 were  
414 discarded due to mismatch of the PET and CRS-R diagnosis, 4 for failure of segmentation  
415 and 2 for head movement artefacts.

#### 416 *MRI Data Acquisition*

417 For the DOC dataset, structural (T1 and DWI) and functional MRI data was acquired on a  
418 Siemens 3T Trio scanner. 3D T1-weighted MP-RAGE images (120 transversal slices,  
419 repetition time = 2300 ms, voxel size = 1.0 x 1.0 x 1.2 mm<sup>3</sup>, flip angle = 9°, field of view = 256  
420 x 256 mm<sup>2</sup>) were acquired prior to the 10 minutes of BOLD fMRI resting-state (i.e. task free)  
421 (EPI, gradient echo, volumes = 300, repetition time = 2000 ms, echo time = 30 ms, flip angle  
422 = 78°, voxel size = 3 x 3 x 3 mm<sup>3</sup>, field of view = 192 x 192 mm<sup>2</sup>, 32 transversal slices). HC  
423 subjects were instructed to keep eyes open and to be in relaxed state during the fMRI data  
424 acquisition. Last, diffusion weighted MRI (DWI) was acquired in 64 directions (b-value = 1,000  
425 s/mm<sup>2</sup>, voxel size = 1.8 x 1.8 x 3.3 mm<sup>3</sup>, field of view 230 x 230 mm<sup>2</sup>, repetition time 5,700  
426 ms, echo time 87 ms, 45 transverse slices, 128 x 128 voxel matrix) preceded by a single  
427 unweighted image (b0).

#### 428 *Resting -state fMRI preprocessing*

429 Preprocessing was performed as in (46) using MELODIC (Multivariate Exploratory Linear  
430 Optimized Decomposition into Independent Components) version 3.14, which is part of  
431 FMRIB's Software Library (FSL, <http://fsl.fmrib.ox.ac.uk/fsl>). The preprocessing consisted of  
432 the following steps: the first five functional images were discarded to reduce scanner  
433 inhomogeneity, motion correction was performed using MCFLIRT, non brain tissue was  
434 removed using Bet Extraction Tool (BET), temporal band-pass filtering with sigma 100  
435 seconds, spatial smoothing was applied using a 5mm FWHM Gaussian kernel, rigid-body  
436 registration was performed, and finally single-session ICA with automatic dimensionality  
437 estimation was employed (51). Then, FIX (FMRIB's ICA-based X-noiseifier) was applied to  
438 remove the noise components and the lesion-driven for each subject. Specifically, FSLeys  
439 in Melodic mode was used to manually identify the single-subject independent components  
440 (ICs) into "good" for cerebral signal, "bad" for noise or injury-driven artifacts, and "unknown"  
441 for ambiguous components. Each component was evaluated based on the spatial map, the  
442 time series, and the temporal power spectrum (51). Next, for each subject, FIX was applied  
443 with default parameters to remove bad and unknown components. Subsequently, the Shen et  
444 al., functional atlas (without cerebellum) was applied for brain parcellation to obtain the BOLD  
445 time series of the 214 cortical and subcortical brain areas in each individual's native EPI  
446 space (30, 52). The cleaned functional data were co-registered to the T1-weighted structural  
447 image by using FLIRT (53). Then, the T1-weighted image was co-registered to the standard  
448 MNI space by using FLIRT (12 DOF), and FNIRT (54). The transformations matrices were  
449 inverted and applied to warp the resting-state atlas from MNI space to the single-subject  
450 functional data using a nearest-neighbor interpolation method to ensure the preservation of  
451 the labels. Finally, the time series for each of the 214 brain areas were extracted using  
452 `fslmaths` and `fslmeants`.

453

454

## 455 *Probabilistic Tractography analysis*

456 A whole-brain structural connectivity (SC) matrix was computed for each subject as reported  
457 in our previous study (46). Briefly, the b0 image was co-registered to the T1 structural image  
458 using FLIRT and the T1 structural image was co-registered to the MNI space using FLIRT and  
459 FNIRT(53, 54). The transformation matrices were inverted and applied to warp the resting-  
460 state atlas from MNI space to the native diffusion space using a nearest-neighbor interpolation  
461 method. Analysis of diffusion images was applied using the FMRIB's Diffusion Toolbox (FDT)  
462 ([www.fmrib.ox.ac.uk/fsl](http://www.fmrib.ox.ac.uk/fsl)). BET was computed, eddy current distortions and head motion were  
463 corrected using eddy correct tool (55). Crossing Fibres were modeled by using BEDPOSTX,  
464 and the probability of multi-fibre orientations was calculated to enhance the sensitivity of non-  
465 dominant fibre populations (56, 57). Then, probabilistic tractography analysis was calculated  
466 in native diffusion space using PROBTRACKX to compute the connectivity probability of each  
467 brain region to each of the other 213 brain regions. Subsequently, the value of each brain area  
468 was divided by its corresponding number of generated tracts to obtain the structural probability  
469 matrix. Finally, the  $SC_{pn}$  matrix was then symmetrized by computing their transpose  $SC_{np}$  and  
470 averaging both matrices.

## 471 *Metastability and time-resolved functional connectivity*

472 BOLD time series for every ROI  $k$  were filtered within the narrowband of 0.01-0.9 Hz. We  
473 estimated both time-resolved functional connectivity and static functional connectivity. Static  
474 functional connectivity ( $FC_{static}$ ) was estimated by the Pearson correlation coefficient between  
475 pairwise narrowband time courses. Time-resolved connectivity was estimated from the  
476 instantaneous phases. The instantaneous phase of the BOLD signal,  $\varphi_k(t)$ , was extracted  
477 from the analytic signal as obtained from the Hilbert transform. The synchronization between  
478 pairs of brain regions was characterised as the difference between their instantaneous  
479 phases. At each time point, the phase difference between two regions  $j$  and  $k$  was used as  
480 estimate for instantaneous phase connectivity  $\Delta\varphi_{jk}(t)$  (58). Evaluation of pairwise connectivity  
481 at each time point resulted in a functional connectivity tensor (number of ROIs x number of  
482 ROIs x time points).

483 Furthermore, we investigated how the synchronization between different nodes fluctuates  
484 across time using the concept of *metastability*. In the current sense, metastability quantifies  
485 how variable the states of phase configurations are as a function of time. We quantified  
486 metastability (i.e. our proxy measure for metastability) in terms of the standard deviation of the  
487 Kuramoto order parameter,  $R(t) = \left| \frac{1}{N} \sum_k^N e^{i\varphi_k(t)} \right|$ , where  $N$  is the number of ROIs and  $i$  denotes  
488 the imaginary unit (59).

489 Similar to (60, 61), we extracted time-evolving networks using non-negative tensor  
490 factorization (NNTF) (62). We used the N-way toolbox (version 1.8) for MATLAB for this  
491 analysis (63). NNTF can be considered as a higher-order principal component analysis. The  
492 goal of the approach is to decompose the functional connectivity tensor  $FC$  into components,  
493 such that the approximation of the functional connectivity tensor  $\widehat{FC}$  can be written as  $\widehat{FC} =$   
494  $\sum_l^L a_l \times b_l \times c_l$ . Here,  $a_l$  and  $b_l$  correspond to vectors decoding spatial information for  
495 component  $l$ , and  $c_l$  represents the vector that contains information on temporal fluctuations  
496 of component  $l$ . Note that the outer product  $a_l \times b_l$  stands for the spatial pattern of functional  
497 connectivity of component  $l$ . The number of components  $L$  can be estimated from the data  
498 using established algorithms (64). However, here, we fixed the number of components based  
499 on the number of *a-priori* expected networks that we were interested in. We fed the NNTF  
500 algorithm with initial conditions for  $a_l$  and  $b_l$  based on the spatial components of six expected  
501 resting-state networks: salience network, fronto-parietal network, default mode network,  
502 subcortical network, sensorimotor network, visual network. We added a residual network to  
503 account for the unexplained variance in the functional connectivity tensor. Note that the spatial

504 initial conditions did not indicate that these spatial components were kept fixed during NNTF  
505 calculation, but these spatial components were free to be adjusted according to maximization  
506 of the explained variance. Data from all subjects and groups were concatenated to allow  
507 convergence to stable results.

### 508 *Relationship between structural eigenmodes and time-resolved functional connectivity*

509 For every subject, we extracted structural eigenmodes from the graph Laplacian  $Q_A$  of the  
510 structural connectivity (SC) matrix defined by  $Q_A = K_{SC} - SC$ , where  $K_{SC}$  refers to the diagonal  
511 degree matrix of SC. We further applied symmetric normalization to obtain a normalized  
512 Laplacian  $Q_{SC}$ . Subsequently, eigenvectors  $u_i$  and eigenvalues (together called eigenmodes)  
513 were extracted using diagonalization of  $Q_{SC}$ , resulting in  $N$  eigenmodes ( $N =$  number of ROIs).  
514 Using a recently introduced approach we mapped functional brain networks at each time point  
515 from the structural eigenmodes (27). In other words, we estimated to what extent functional  
516 connectivity at each time point  $FC(t)$  could be explained by a linear combination of the  
517 eigenmodes

$$518 \quad FC(t) \approx K_{FC}(t) - K_{FC}^{\frac{1}{2}}(t)(UP(t)U^T)K_{FC}^{\frac{1}{2}}(t), \quad (1)$$

519 where  $K_{FC}(t)$  is the diagonal node strength matrix of the functional connectivity matrix  $FC(t)$   
520 at time  $t$ . The matrix  $P(t)$  corresponds to the weighting coefficient matrix for the eigenmodes  
521 and is obtained after optimisation and equal to

$$522 \quad P(t) = \text{diag}(u_1^T Q_{FC}(t) u_1, \dots, u_N^T Q_{FC}(t) u_N). \quad (2)$$

523 Hence, modulations of eigenmode expressions over time are expressed in  $P(t)$ . Here,  $Q_{FC}(t)$   
524 is the normalised graph Laplacian of  $FC(t)$  at time  $t$ , and  $u_i$  is the  $i$ -th eigenvector of  $Q_{SC}$  and  
525 the  $i$ -th column of  $U$ .

### 526 *Analysis steps*

527 1. *Time-resolved functional connectivity.* Individual temporal time courses  $c_l^{ind}$  for  
528 expression of component  $l$  for every subject were extracted from  $c_l$ . A high value of  $c_l$   
529 at a certain time point indicates strong expression of this spatial pattern of functional  
530 connectivity ( $a_l \times b_l$ ) at that time point. At each time point we determined the  
531 component with the strongest expression ( $\max(c_l^{ind})$ ), and assumed that connectivity  
532 at that point in time was dominated by this state or component. The duration that this  
533 component retained the strongest expression was considered as state duration or  
534 dwell time (see Figure 1). In addition, we also characterized the amount of  
535 nonstationarity in  $c_l$  (31, 65), i.e. excursions from the median. The rationale for using  
536 this metric is its sensitivity to detect modulations if the underlying system is indeed  
537 dynamic (65). Mann-Whitney U tests were used to test, for each network separately,  
538 differences in state durations and excursion from the median between groups.

539 2. *Structural vs functional brain networks.* We first estimated the relationship between  
540 static functional connectivity and the structural connectivity itself (without decomposing  
541 SC into eigenmodes). This relationship was estimated in terms of a Pearson correlation  
542 coefficient between the SC and  $FC_{\text{static}}$ , denoted as  $\text{corr}(FC_{\text{static}}, SC)$ . We secondly  
543 analysed the amount to which time-varying functional networks could be explained by  
544 expressions of the structural eigenmodes. We therefore computed the Pearson  
545 correlation between the empirical  $FC(t)$  and the eigenmode predicted  $FC(t)$ , denoted  
546 as  $\text{corr}(FC, \text{eigenmodes})$ . In order to be able to test whether there was a difference in  
547 fluctuations of eigenmode expression over time between groups, we quantified the  
548 eigenmode modulation strength defined as  $\Delta_{\text{eigenmode}} = \sum_{t_k=1, t_l=1}^{T, T} \|P(t_k) - P(t_l)\|$ ,  
549 where  $t_j$  and  $t_k$  correspond to different points in time and  $T$  to total duration of the

550 recording. As the first eigenmodes can be considered as dominant eigenmodes and  
551 more important to shape functional brain networks (25), we evaluated the eigenmode  
552 modulation strength for the dominant eigenmodes  $i = \{1, \dots, N/2\}$  and non-  
553 dominant eigenmodes  $i = \{N/2, \dots, N\}$  separately. We further computed the correlation  
554 between eigenmode modulation strength and metastability in all groups separately in  
555 order to test whether modulations in eigenmode expression related to our proxy  
556 measure for metastability. Group differences for all metrics was tested using Mann-  
557 Whitney U tests.

558 In order to test whether eigenmode predictions of functional connectivity could be  
559 obtained by chance, we created surrogate data and redid analysis for the surrogate  
560 data. Surrogate data for fMRI BOLD time series were obtained using the circular time  
561 shifted method (66). Time-resolved phase connectivity was estimated in the same way  
562 as for genuine empirical data. Time-resolved connectivity obtained from surrogate data  
563 was subsequently predicted using the eigenmodes.

564 False discovery rate was used to correct for multiple comparisons for analysis steps 1  
565 and 2: number of metrics (excursions \* seven networks, dwell time \* seven networks,  
566 metastability,  $\text{corr}(\text{FC}_{\text{static}}, \text{SC})$ ,  $\text{corr}(\text{FC}, \text{eigenmodes})$ , non-dominant and dominant  
567 eigenmodes)\* 3 comparisons + surrogate comparison with genuine data 3 \* 3,  
568 ( $\text{corr}(\text{FC}, \text{eigenmodes})$ , non-dominant and dominant eigenmodes) comparisons = 66  
569 tests) (67).

570 3. *Classification Algorithm.* For two group classifications (i.e., UWS vs MCS, UWS vs HC,  
571 MCS vs HC), a two class “linear SVM” model with 2<sup>nd</sup> order polynomial kernel was  
572 employed. To train the classifier, we used the “fitsvm” function and to test the classifier  
573 performance, we used the “SVMModel.predict” function of MATLAB. As we have a low  
574 sample size, we employed three popular algorithms to avoid model or parameter bias.  
575 We employed the SVM model with: 1) Leave-one-out cross-validation (LOOCV); 2) 10-  
576 fold cross validation and 3) splitting the data in 60-40%. Furthermore, classification  
577 performance was verified with real and surrogate data features to get an estimate of  
578 the bias in the results obtained with the real data. The discriminative and the predictive  
579 capabilities of the classifier were evaluated with measures obtained from receiver  
580 operating curves (ROC): accuracy, sensitivity, specificity (68).

581 4. *Feature Ranking.* To understand which features predominantly contribute to classify the  
582 UWS from MCS, and healthy controls from patients, we used the classification-based  
583 feature weighting algorithm based on diagonal adaptation of neighbourhood  
584 component analysis (NCA). We used the ‘fscnca’ function of MATLAB that learns the  
585 feature weights using a diagonal adaptation of NCA and returns the weight for each  
586 functional dynamic and structural-functional feature (69).

587

## 588 V. References

- 589 1. S. Laureys, *et al.*, Unresponsive wakefulness syndrome: a new name for the  
590 vegetative state or apallic syndrome. *BMC Med.* **8**, 1–4 (2010).
- 591 2. J. T. Giacino, *et al.*, The minimally conscious state: definition and diagnostic criteria.  
592 *Neurology* **58**, 349–353 (2002).
- 593 3. C. Schnakers, *et al.*, The Nociception Coma Scale: a new tool to assess nociception  
594 in disorders of consciousness. *Pain* **148**, 215–219 (2010).
- 595 4. B. L. Edlow, J. Claassen, N. D. Schiff, D. M. Greer, Recovery from disorders of  
596 consciousness: mechanisms, prognosis and emerging therapies. *Nat. Rev. Neurol.*,  
597 1–22 (2020).
- 598 5. E. Amico, *et al.*, Mapping the functional connectome traits of levels of consciousness.  
599 *Neuroimage* **148**, 201–211 (2017).
- 600 6. L. Heine, *et al.*, Resting state networks and consciousness. *Front. Psychol.* **3**, 295  
601 (2012).
- 602 7. A. Demertzi, *et al.*, Intrinsic functional connectivity differentiates minimally conscious  
603 from unresponsive patients. *Brain* **138**, 2619–2631 (2015).
- 604 8. E. A. Fridman, B. J. Beattie, A. Broft, S. Laureys, N. D. Schiff, Regional cerebral  
605 metabolic patterns demonstrate the role of anterior forebrain mesocircuit dysfunction  
606 in the severely injured brain. *Proc. Natl. Acad. Sci.* **111**, 6473–6478 (2014).
- 607 9. S. Laureys, *et al.*, Restoration of thalamocortical connectivity after recovery from  
608 persistent vegetative state. *Lancet* **355**, 1790–1791 (2000).
- 609 10. A. Demertzi, A. Soddu, S. Laureys, Consciousness supporting networks. *Curr. Opin.*  
610 *Neurobiol.* **23**, 239–244 (2013).
- 611 11. J. T. Giacino, J. J. Fins, S. Laureys, N. D. Schiff, Disorders of consciousness after  
612 acquired brain injury: the state of the science. *Nat. Rev. Neurol.* **10**, 99 (2014).
- 613 12. P. Barttfeld, *et al.*, Signature of consciousness in the dynamics of resting-state brain  
614 activity. *Proc. Natl. Acad. Sci.* **112**, 887–892 (2015).
- 615 13. A. I. Luppi, *et al.*, Consciousness-specific dynamic interactions of brain integration  
616 and functional diversity. *Nat. Commun.* **10**, 1–12 (2019).
- 617 14. A. Demertzi, *et al.*, Human consciousness is supported by dynamic complex patterns  
618 of brain signal coordination. *Sci. Adv.* **5**, eaat7603 (2019).
- 619 15. L. E. Suárez, R. D. Markello, R. F. Betzel, B. Misic, Linking structure and function in  
620 macroscale brain networks. *Trends Cogn. Sci.* (2020).
- 621 16. A. Avena-Koenigsberger, B. Misic, O. Sporns, Communication dynamics in complex  
622 brain networks. *Nat. Rev. Neurosci.* **19**, 17 (2018).
- 623 17. Y. Sanz Perl, *et al.*, Perturbations in dynamical models of whole-brain activity  
624 dissociate between the level and stability of consciousness. *PLoS Comput. Biol.* **17**,  
625 e1009139 (2021).

- 626 18. D. Golkowski, *et al.*, Dynamic Patterns of Global Brain Communication Differentiate  
627 Conscious From Unconscious Patients After Severe Brain Injury. *Front. Syst.*  
628 *Neurosci.* **15** (2021).
- 629 19. S. M. Del Pozo, *et al.*, Unconsciousness reconfigures modular brain network  
630 dynamics. *Chaos An Interdiscip. J. Nonlinear Sci.* **31**, 93117 (2021).
- 631 20. B. Cao, *et al.*, Abnormal dynamic properties of functional connectivity in disorders of  
632 consciousness. *NeuroImage Clin.* **24**, 102071 (2019).
- 633 21. J. Rizkallah, *et al.*, Decreased integration of EEG source-space networks in disorders  
634 of consciousness. *NeuroImage Clin.* **23**, 101841 (2019).
- 635 22. M. M. Monti, *et al.*, Thalamo-frontal connectivity mediates top-down cognitive  
636 functions in disorders of consciousness. *Neurology* **84**, 167–173 (2015).
- 637 23. G. Deco, *et al.*, Resting-state functional connectivity emerges from structurally and  
638 dynamically shaped slow linear fluctuations. *J. Neurosci.* **33**, 11239–11252 (2013).
- 639 24. G. Deco, M. L. Kringelbach, Metastability and coherence: extending the  
640 communication through coherence hypothesis using a whole-brain computational  
641 perspective. *Trends Neurosci.* **39**, 125–135 (2016).
- 642 25. S. Atasoy, I. Donnelly, J. Pearson, Human brain networks function in connectome-  
643 specific harmonic waves. *Nat. Commun.* **7** (2016).
- 644 26. P. A. Robinson, *et al.*, Eigenmodes of brain activity: Neural field theory predictions  
645 and comparison with experiment. *Neuroimage* **142**, 79–98 (2016).
- 646 27. P. Tewarie, *et al.*, Mapping functional brain networks from the structural connectome:  
647 relating the series expansion and eigenmode approaches. *Neuroimage* **216**, 116805  
648 (2020).
- 649 28. S. Atasoy, G. Deco, M. L. Kringelbach, J. Pearson, Harmonic brain modes: a unifying  
650 framework for linking space and time in brain dynamics. *Neurosci.* **24**, 277–293  
651 (2018).
- 652 29. M. G. Preti, D. Van De Ville, Decoupling of brain function from structure reveals  
653 regional behavioral specialization in humans. *Nat. Commun.* **10**, 1–7 (2019).
- 654 30. E. S. Finn, *et al.*, Functional connectome fingerprinting: identifying individuals using  
655 patterns of brain connectivity. *Nat. Neurosci.* **18**, 1664–1671 (2015).
- 656 31. A. Zalesky, A. Fornito, L. Cocchi, L. L. Gollo, M. Breakspear, Time-resolved resting-  
657 state brain networks. *Proc. Natl. Acad. Sci.* **111**, 10341–10346 (2014).
- 658 32. N. D. Schiff, Recovery of consciousness after brain injury: a mesocircuit hypothesis.  
659 *Trends Neurosci.* **33**, 1–9 (2010).
- 660 33. S. Dehaene, J.-P. Changeux, L. Naccache, The global neuronal workspace model of  
661 conscious access: from neuronal architectures to clinical applications. *Charact.*  
662 *Conscious. From Cogn. to Clin.*, 55–84 (2011).
- 663 34. H. Blumenfeld, Brain mechanisms of conscious awareness: Detect, pulse, switch, and  
664 wave. *Neurosci.*, 10738584211049378 (2021).

- 665 35. L. Naccache, Minimally conscious state or cortically mediated state? *Brain* **141**, 949–  
666 960 (2018).
- 667 36. J. S. Crone, B. J. Bio, P. M. Vespa, E. S. Lutkenhoff, M. M. Monti, Restoration of  
668 thalamo-cortical connectivity after brain injury: recovery of consciousness, complex  
669 behavior, or passage of time? *J. Neurosci. Res.* **96**, 671–687 (2018).
- 670 37. J. Annen, *et al.*, Function–structure connectivity in patients with severe brain injury as  
671 measured by MRI-DWI and FDG-PET. *Hum. Brain Mapp.* **37**, 3707–3720 (2016).
- 672 38. L. Weng, *et al.*, Abnormal structural connectivity between the basal ganglia, thalamus,  
673 and frontal cortex in patients with disorders of consciousness. *Cortex* **90**, 71–87  
674 (2017).
- 675 39. G. A. Mashour, P. Roelfsema, J.-P. Changeux, S. Dehaene, Conscious processing  
676 and the global neuronal workspace hypothesis. *Neuron* **105**, 776–798 (2020).
- 677 40. F. Cavanna, M. G. Vilas, M. Palmucci, E. Tagliazucchi, Dynamic functional  
678 connectivity and brain metastability during altered states of consciousness.  
679 *Neuroimage* **180**, 383–395 (2018).
- 680 41. J. Stender, *et al.*, Diagnostic precision of PET imaging and functional MRI in disorders  
681 of consciousness: a clinical validation study. *Lancet* **384**, 514–522 (2014).
- 682 42. W. S. van Erp, *et al.*, Unexpected emergence from the vegetative state: delayed  
683 discovery rather than late recovery of consciousness. *J. Neurol.* **266**, 3144–3149  
684 (2019).
- 685 43. D. A. Engemann, *et al.*, Robust EEG-based cross-site and cross-protocol  
686 classification of states of consciousness. *Brain* **141**, 3179–3192 (2018).
- 687 44. D. Candia-Rivera, *et al.*, Neural Responses to Heartbeats Detect Residual Signs of  
688 Consciousness during Resting State in Postcomatose Patients. *J. Neurosci.* **41**,  
689 5251–5262 (2021).
- 690 45. A. Thibaut, *et al.*, Preservation of brain activity in unresponsive patients identifies  
691 MCS star. *Ann. Neurol.* **90**, 89–100 (2021).
- 692 46. A. López-González, *et al.*, Loss of consciousness reduces the stability of brain hubs  
693 and the heterogeneity of brain dynamics. *Commun. Biol.* **4**, 1–15 (2021).
- 694 47. P. Tewarie, *et al.*, How do spatially distinct frequency specific MEG networks emerge  
695 from one underlying structural connectome? The role of the structural eigenmodes.  
696 *Neuroimage* **186**, 211–220 (2019).
- 697 48. A. Hillebrand, *et al.*, Detecting epileptiform activity from deeper brain regions in  
698 spatially filtered MEG data. *Clin. Neurophysiol. Off. J. Int. Fed. Clin. Neurophysiol.*  
699 **127**, 2766–2769 (2016).
- 700 49. R. Panda, *et al.*, Posterior integration and thalamo-frontotemporal broadcasting are  
701 impaired in disorders of consciousness (2021).
- 702 50. J. T. Giacino, K. Kalmar, J. Whyte, The JFK Coma Recovery Scale-Revised:  
703 measurement characteristics and diagnostic utility. *Arch. Phys. Med. Rehabil.* **85**,  
704 2020–2029 (2004).

- 705 51. L. Griffanti, *et al.*, ICA-based artefact removal and accelerated fMRI acquisition for  
706 improved resting state network imaging. *Neuroimage* **95**, 232–247 (2014).
- 707 52. X. Shen, F. Tokoglu, X. Papademetris, R. T. Constable, Groupwise whole-brain  
708 parcellation from resting-state fMRI data for network node identification. *Neuroimage*  
709 **82**, 403–415 (2013).
- 710 53. M. Jenkinson, S. Smith, A global optimisation method for robust affine registration of  
711 brain images. *Med. Image Anal.* **5**, 143–156 (2001).
- 712 54. J. L. R. Andersson, M. Jenkinson, S. Smith, Non-linear registration, aka Spatial  
713 normalisation FMRIB technical report TR07JA2. *FMRIB Anal. Gr. Univ. Oxford* **2**, e21  
714 (2007).
- 715 55. J. L. R. Andersson, S. N. Sotiropoulos, An integrated approach to correction for off-  
716 resonance effects and subject movement in diffusion MR imaging. *Neuroimage* **125**,  
717 1063–1078 (2016).
- 718 56. T. E. J. Behrens, *et al.*, Characterization and propagation of uncertainty in diffusion-  
719 weighted MR imaging. *Magn. Reson. Med. An Off. J. Int. Soc. Magn. Reson. Med.* **50**,  
720 1077–1088 (2003).
- 721 57. T. E. J. Behrens, H. J. Berg, S. Jbabdi, M. F. S. Rushworth, M. W. Woolrich,  
722 Probabilistic diffusion tractography with multiple fibre orientations: What can we gain?  
723 *Neuroimage* **34**, 144–155 (2007).
- 724 58. E. Glerean, J. Salmi, J. M. Lahnakoski, I. P. Jääskeläinen, M. Sams, Functional  
725 magnetic resonance imaging phase synchronization as a measure of dynamic  
726 functional connectivity. *Brain Connect.* **2**, 91–101 (2012).
- 727 59. G. Deco, M. L. Kringelbach, V. K. Jirsa, P. Ritter, The dynamics of resting fluctuations  
728 in the brain: metastability and its dynamical cortical core. *Sci. Rep.* **7**, 3095 (2017).
- 729 60. A. Ponce-Alvarez, *et al.*, Resting-state temporal synchronization networks emerge  
730 from connectivity topology and heterogeneity. *PLoS Comput. Biol.* **11**, e1004100  
731 (2015).
- 732 61. P. Tewarie, *et al.*, Tracking dynamic brain networks using high temporal resolution  
733 MEG measures of functional connectivity. *Neuroimage* **200**, 38–50 (2019).
- 734 62. R. Bro, PARAFAC. Tutorial and applications. *Chemom. Intell. Lab. Syst.* **38**, 149–171  
735 (1997).
- 736 63. C. A. Andersson, R. Bro, The N-way toolbox for MATLAB. *Chemom. Intell. Lab. Syst.*  
737 **52**, 1–4 (2000).
- 738 64. M. E. Timmerman, H. A. L. Kiers, Three-mode principal components analysis:  
739 Choosing the numbers of components and sensitivity to local optima. *Br. J. Math.*  
740 *Stat. Psychol.* **53**, 1–16 (2000).
- 741 65. R. Hindriks, *et al.*, Can sliding-window correlations reveal dynamic functional  
742 connectivity in resting-state fMRI? *Neuroimage* **127**, 242–256 (2016).
- 743 66. R. Q. Quiroga, A. Kraskov, T. Kreuz, P. Grassberger, Performance of different  
744 synchronization measures in real data: a case study on electroencephalographic

- 745 signals. *Phys. Rev. E* **65**, 41903 (2002).
- 746 67. Y. Benjamini, Y. Hochberg, Controlling the false discovery rate: a practical and  
747 powerful approach to multiple testing. *J. R. Stat. Soc. Ser. B*, 289–300 (1995).
- 748 68. R. D. Bharath, *et al.*, Machine learning identifies “rsfMRI epilepsy networks” in  
749 temporal lobe epilepsy. *Eur. Radiol.* **29**, 3496–3505 (2019).
- 750 69. H. Eryilmaz, *et al.*, Working memory load-dependent changes in cortical network  
751 connectivity estimated by machine learning. *Neuroimage* **217**, 116895 (2020).
- 752
- 753
- 754
- 755
- 756

## 757 VI. Figures

758 **Figure 1: Overview of the analysis pipeline.** We used the same Shen parcellation for DWI  
759 and fMRI data. Time-resolved functional connectivity was estimated using a metric for phase  
760 connectivity. A proxy measure for metastability was derived from the phase information. Time-  
761 resolved networks were subsequently extracted from the concatenated data from all subjects  
762 using non-negative tensor factorisation (NNTF). Dwell times and nonstationarity (excursions  
763 from the median) were retrieved for each spatial pattern of functional connectivity (6 resting-  
764 state networks and 1 'residual' network). At the same time, time-resolved connectivity was  
765 predicted on a sample by sample basis based on a linear combination of eigenmodes (hidden  
766 patterns in the anatomical network). Measures were used for classification and feature  
767 ranking.

768 **Figure 2: Metastability and time-resolved functional networks in DOC.** Panel A displays  
769 metastability for all groups: healthy controls (HC), minimally conscious state (MCS),  
770 unresponsive wakefulness state (UWS). Panels B-H display the distributions of nonstationarity  
771 (excursions from the median) for the residuals and time-resolved networks. Panels I-N show  
772 the spatial patterns of time-resolved output networks. Abbreviations: default mode network  
773 (DMN), frontoparietal network (FPN), \*\*, and \*\*\* denote  $p < 0.01$  and  $p < 0.001$  respectively.  
774 The colourbar indicates the strength of that specific area to the overall spatial pattern.

775 **Figure 3: Relationship between time-resolved connectivity and eigenmodes.** Panel A  
776 shows the prediction of static functional connectivity based on structural connectivity for all  
777 three groups (HC, MCS and UWS) in terms of the Pearson correlation coefficient. Panel B  
778 shows the prediction of time-resolved functional connectivity based on eigenmodes. These  
779 distributions of eigenmode predictions are accompanied with predictions based on surrogate  
780 data. We further illustrate the level of fluctuations in eigenmode expression for all three groups  
781 (HC, MCS, UWS) for dominant (reflecting network integration, Panel C) and non-dominant  
782 eigenmodes (reflecting increasing network segregation, Panel D) accompanied with results  
783 for surrogate data, \*\* and \*\*\* denote  $p < 0.01$  and  $p < 0.001$  respectively. Panels E-G show  
784 that metastability is strongly correlated to modulations in eigenmode expression within every  
785 group.

786 **Figure 4: Feature ranking.** We illustrate the feature weights for classification based on  
787 diagonal adaptation of neighborhood component analysis (NCA).

788

789

790

791

792

793

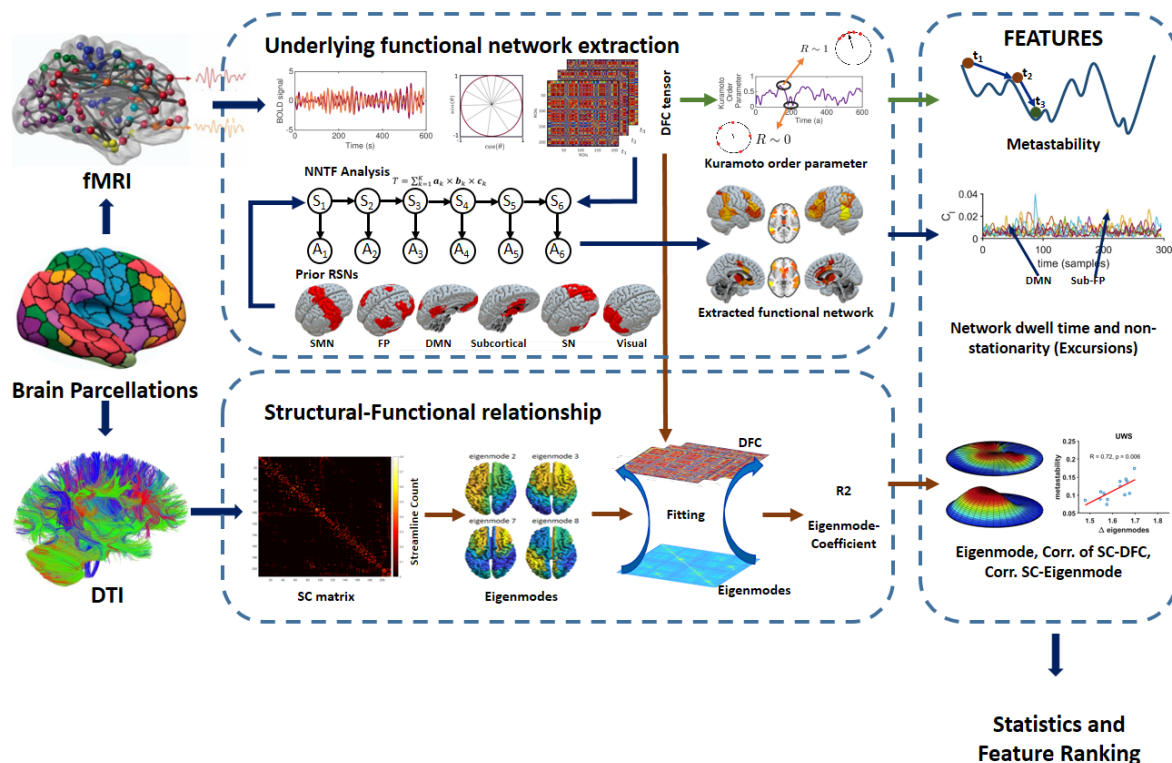
794

795

796

797

798 Figure 1:



799

800

801

802

803

804

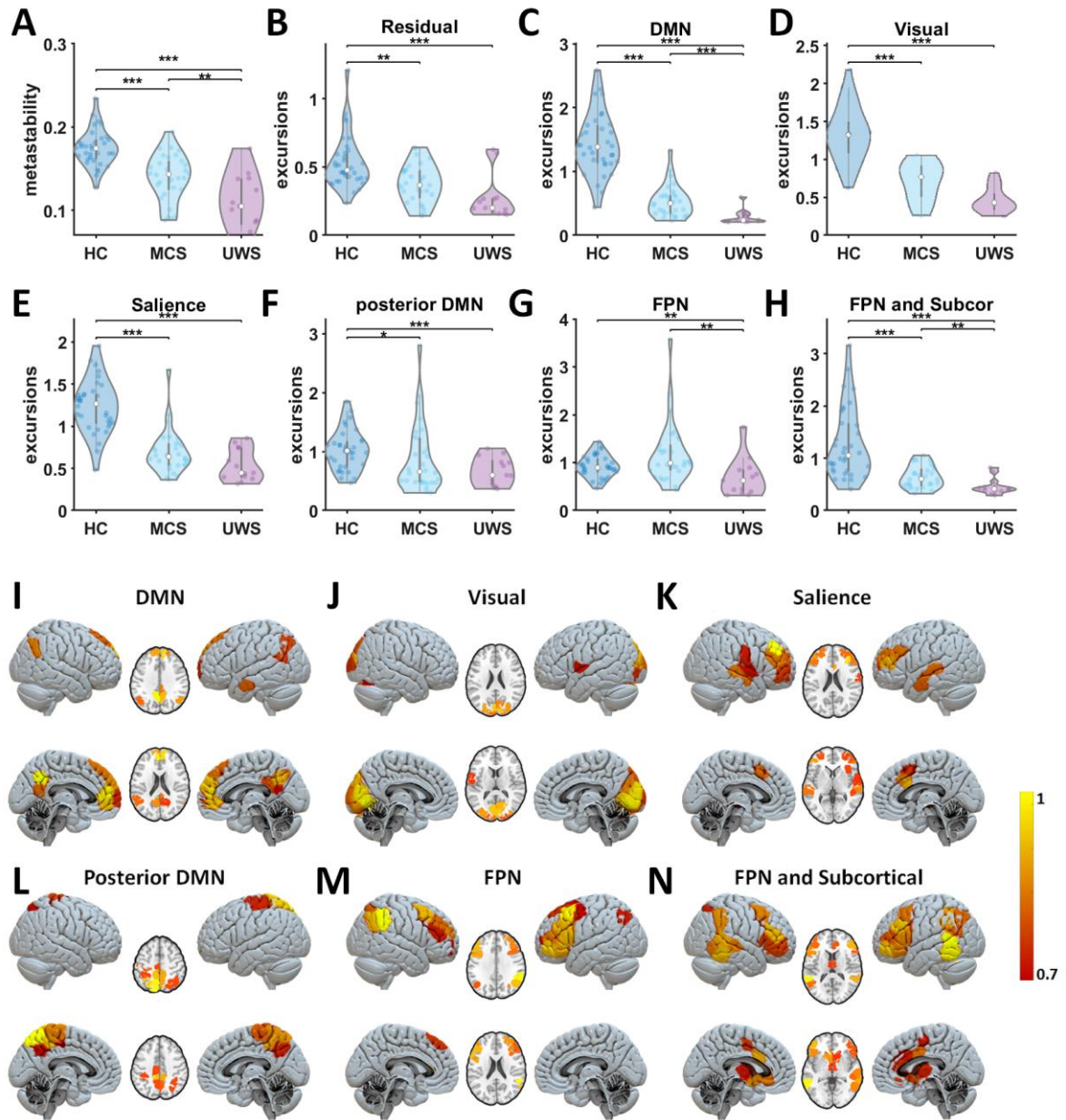
805

806

807

808

809 Figure 2:



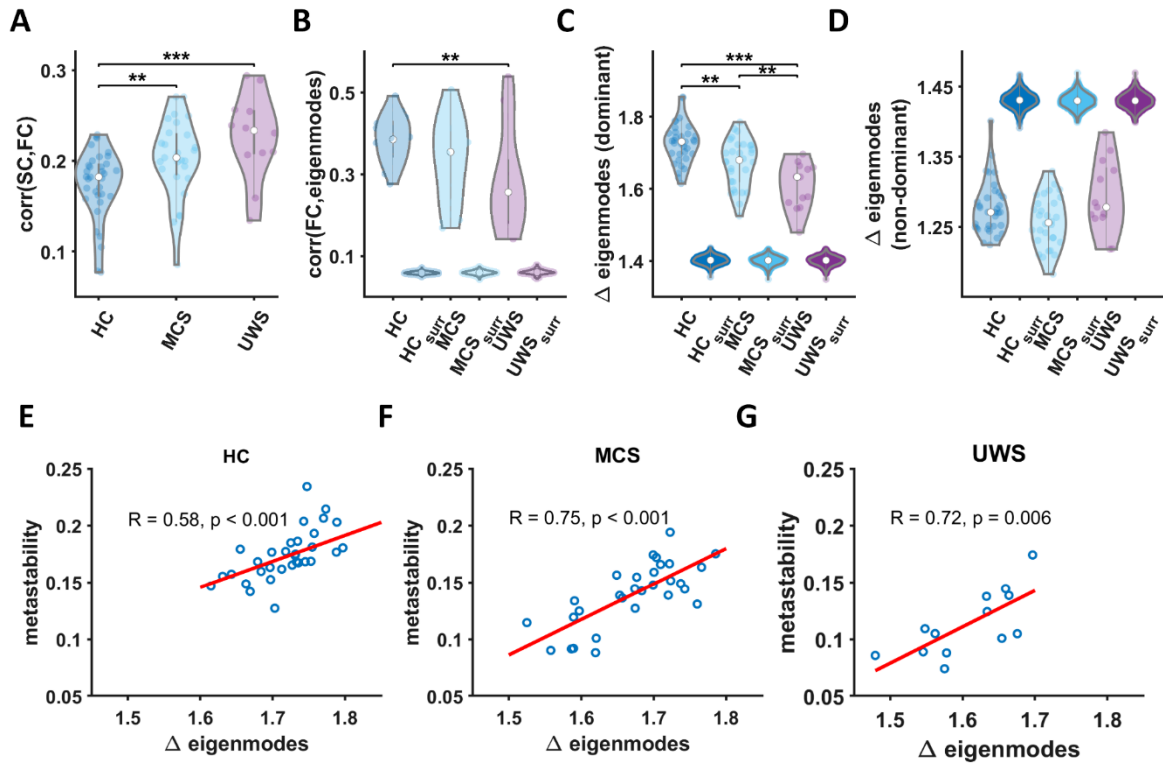
810

811

812

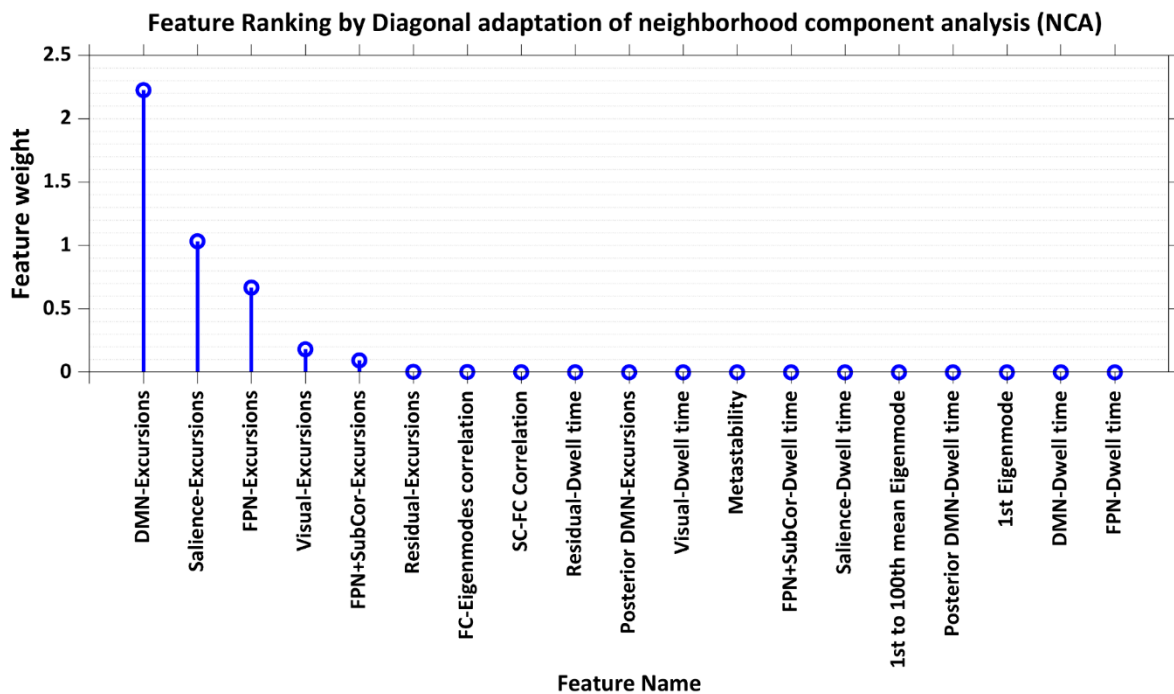
813 Figure 3:

814



815

816 Figure 4:



817

818

819 Table 1. Classification accuracy, sensitivity and specificity (mean and standard deviation) for  
 820 MCS vs UWS, HC vs UWS and HC vs MCS using three different SVM-based classification  
 821 approaches. Performance of the classification using the real experimental data is presented  
 822 alongside the performance of classification based on surrogate data, to define change level.

SVM classification method	Group Comparison	Accuracy		Sensitivity		Specificity	
		Experimental data	Surrogate data	Experimental data	Surrogate data	Experimental data	Surrogate data
LOOCV (Leave-one-out cross-validation)	MCS vs UWS	79.1%	66%	83.3%	100%	69.2%	0%
	HC vs UWS	95.8%	72%	97.1%	100%	92.3%	0%
	HC vs MCS	95.3%	53%	94.1%	100%	96.7%	0%
10-fold cross-validation	MCS vs UWS	76.1±0.03%	66±0%	80.0±0.04%	100±0%	67.1±0.04%	0±0%
	HC vs UWS	95.5±0.01%	72±0%	96.6±0.01%	100±0%	92.8±0.04%	0±0%
	HC vs MCS	93.8±0.02%	53±0%	93.8±0.01%	100±0%	93.7±0.03%	0±0%
60-40 data splitting	MCS vs UWS	73.5±0.12%	66±0%	78.4±0.14%	100±0%	64.5±0.11%	0±0%
	HC vs UWS	95.5±0.05%	72±0%	96.3±0.07%	100±0%	93.4±0.08%	0±0%
	HC vs MCS	93.6±0.05%	53±0%	93.3±0.06%	100±0%	94.2±0.08%	0±0%

823

824

825